Hindawi
Shock and Vibration
Volume 2019, Article ID 2631592, 10 pages
https://doi.org/10.1155/2019/2631592

Research Article

Quantitative Precursory Information of Weak Shocking Failures of Composite Soft Roof

Lihua Wang[1], **Zenghui Zhao**[2], **Zhongxi Tian**[3] **and Wei Sun**[2]

[1]*Shandong Key Laboratory of Civil Engineering Disaster Prevention and Mitigation, Shandong University of Science and Technology, Qingdao 266590, China*
[2]*State Key Laboratory of Mining Disaster Prevention and Control Co-Founded by Shandong Province and the Ministry of Science and Technology, Shandong University of Science and Technology, Qingdao 266590, China*
[3]*College of Architecture and Civil Engineering, Liaocheng University, Liaocheng 252000, China*

Correspondence should be addressed to Zenghui Zhao; tgzyzzh@163.com

Received 2 November 2018; Accepted 29 January 2019; Published 17 February 2019

Academic Editor: Shuaishuai Sun

To reveal the mechanism of weak roof shocking in mine roadway arranged in weakly consolidated soft rock strata commonly observed in western China, a bearing system of composite roof composed of weakly consolidated soft rocks and coal layers was proposed. Then, theoretical analysis and numerical calculation were applied for instability failures of the mass bearing system with strong body and weak body. Eventually, precursory information and criteria of instability failures of the bearing system were developed. The main conclusions obtained are as follows: (1) as the elastic energy released at the postpeak failure stage of weak body contributes to system failures, the equivalent stiffness for system failures consists of the stiffness of strong body and the deterioration stiffness of weak body at softening stage; (2) during the loading process of the two-body system, isochronous sudden jumps of the deformation rate in either body can be regarded as the precursory information of weak impact failures; (3) the frequency of sudden jumps of deformation rate is significantly related to the stiffness, indicating that weak impact failures are readily observed in composite soft roof as stiffnesses of weakly consolidated soft rocks and coal seam are close to each other. This study provides references for prevention and control of weak shocking disasters of composite roofs in western China.

1. Introduction

Underground rock formations in underground construction and mining engineering can be regarded as composite structures with different geological bodies as dynamic disasters such as bursts in rocks and coal roadways caused by excavation, and mining disturbances are indeed results of instability deformations of composite structures caused by interactions of geological bodies with different mechanical properties [1–3]. In underground tunnels, a composite load-bearing system consisting of roof, coal seam, and floor is observed, and instability of any body may cause the failures of the entire system. Due to differences in strength, stiffness, and lithology of different geological bodies, the failure characteristics of the composite body are completely different from that of any single body. The structural effect dominates mechanical behaviors of the composite system. Therefore, it is of great significance to understand the overall mechanical effect and failure precursory information of rock-coal composite structures in order to predict dynamic disasters in mining.

In recent years, researchers have studied the failure characteristics of combined models of different geological bodies by traditional mechanical tests. For instance, the postpeak stability of two-body systems consisting of roof and coal was investigated [4]. Based on the microfractures in the evolution of earthquake in two-body models, precursory principles of deformation localization and elastic rebound were clarified [5, 6]. In terms of coal-rock composite structures, mechanical properties and dynamic failure characteristics of coal-rock body with different height ratios were studied experimentally [7–9], and a nonlinear model to describe overall failures was established [10]. Some researchers claimed that failures of coal-rock body may be attributed to contribution of energy accumulated in rock to failures of coal

unit during loading [11–13]. These results indicated that dynamic instability of coal rocks is a disaster of instability of surrounding rock-coal systems. Hence, for roof-coal-floor systems, interactions of subsystems such as roof, coal seam, and floor should be taken into full consideration in order to investigate the overall effects of subsystems and composite system on the dynamic instability tendency from the aspects of storage and release of deformation energy in coal and rock mass. However, it is difficult for traditional methods to effectively obtain the instability characteristics and precursor information of the composite body. Therefore, the precursor of coal sample destruction was further studied by comprehensive monitoring methods, including infrared radiation and acoustic emission. Other studies indicated that the thermal effect is proportional to strength of microfracture of coal samples, and the temperature effect of infrared radiation was maximized at loading = 70% of the coal sample strength [14–16]. Also, preliminary observations on the infrared radiation information produced by deformation and breakdown of the coal were obtained according to this principle [17, 18]. The results revealed that the ultimate failure precursor of the burst tendency of coal sample body under was approximately at $0.90\sigma_c$ and $0.81\sigma_c$ under uniaxial loading and cyclic loading, respectively. Based on that, compression tests of sandstone-coal body and sandstone-coal-mudstone body were performed using a synchronous device consisting of infrared imaging system and emission monitoring system. The quantitative precursory locations of instability failure of composite structures were captured by thermal infrared and acoustic emission, and the results showed that the instability precursor of the three-body model was behind that of the two-body model [19, 20].

The studies mentioned above demonstrated that underground engineering disasters are reflections of overall instability of composite structure systems with different geological bodies during mining disturbance. Currently, researchers have carried out various theoretical and experimental studies on the instability failure and rock burst of coal-rock systems in mining engineering, and both qualitative and quantitative criteria of instability failures of combination body have been proposed to facilitate prediction and prevention of dynamic instability disasters. However, these conclusions were obtained based on hard rock-soft coal systems, and it is not applicable to weakly cemented soft rock strata. Moreover, the precursory information of instability failures was mostly qualitative, and acquisition of quantitative information was extremely complicated. It has been demonstrated that instability fractures of weakly consolidated rock sample do not occur at the peak. Instead, it is commonly observed at a certain position during the postpeak softening stage, and such instability points are readily observed in weak rock burst [21–24]. Also, release of elastic energy was observed in rock mass during the postpeak softening stage.

For this reason, instability failure characteristics of strong-weak geological system with different stiffness were discussed according to the combined surrounding rock system with strain softening rock strata and coal seams. Quantitative criteria of instability failure characteristics of such structures were proposed based on theoretical analysis and numerical simulation. Additionally, the relevant conclusions are applied in engineering practice to provide references for prevention and control of weak roof shocking disasters in mining engineering in western China.

2. Mechanism of Instability Failures of Strong-Weak Geological System with Strain-Softening Behaviors

2.1. Model of Strong-Weak Geological Body. Disasters such as rock burst are results of instability deformations and failures of mechanical system composed of different geological bodies that interact with each other. Owing to the differences in lithologies of different geological bodies, weak parts are observed in the system. Under stresses or disturbance conditions, weak body was destroyed first, resulting in energy release from surrounding bodies and then failures. Even in weak cemented soft rock strata, weak shocking failures of weak surrounding rocks and coal mass were observed, accompanied by hissing crackle sounds. Such failures are caused by interactions of strain-softening materials with varying strength and stiffness. According to the stiffness criteria proposed by Cook [25], the instability failure of the weak body was initiated at the postpeak stress decreasing stage, and strain-softening of rock mass is prerequisite for sudden catastrophic damages.

Figure 1 shows the strong-weak geological system, and both bodies exhibit strain-softening behaviors. The stiffnesses of strong and weak body at the prestage are defined as K_s and K_w, respectively. Under axial force (F_1), displacements of the strong body and the weak body were η_s and η_w, respectively. Therefore, the overall displacement of the system can be expressed as

$$\eta_t = \eta_s + \eta_w. \tag{1}$$

Figure 2 shows the load-displacement curves of the two bodies during loading. The load-displacement can be expressed as [26]

$$\begin{cases} F_s = K_s\eta_s, & \eta_s < \eta_{sp}, \\ F_s = K_s\eta_s \exp\left[-\left(\dfrac{\eta_s}{\eta_{sc}}\right)^m\right], & \eta_s \geq \eta_{sp}, \end{cases}$$
$$\begin{cases} F_w = K_w\eta_w, & \eta_w < \eta_{wp}, \\ F_w = K_w\eta_w \exp\left[-\left(\dfrac{\eta_w}{\eta_{wc}}\right)^n\right], & \eta_w > \eta_{wp}, \end{cases} \tag{2}$$

where F_s and F_w refer to the axial loads on strong body and weak body, respectively. η_{sc} and η_{wc} refer to the axial displacements of strong body and weak body, respectively, at peak loading, and they are related to their peak strengths. η_{sp} and η_{wp} refer to the displacements of strong body and weak body, respectively, at yielding point. m and n refer to fitting parameters.

In the quasistatic loading process, the system is in equilibrium and the following relation should be satisfied before catastrophic damages in weak body:

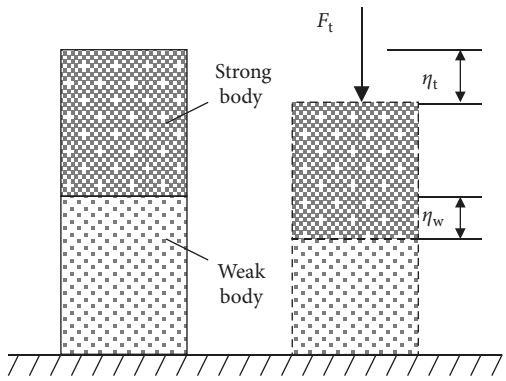

Figure 1: Strong-weak geological system.

$$F_t(\eta_t) = F_s(\eta_s) = F_w(\eta_w). \tag{3}$$

2.2. Energy Evolution Mechanism in Loading Process. Before peak loading of the weak body, the system is in elastic stage with no damages, if the relatively short yield stage is not taken into consideration. In this case, the two bodies are in a state of energy accumulation due to elastic deformations. At peak loading of the weak body, internal damages caused by propagation of microcracks were observed. At postpeak loading process, the energy consumed by damages of the weak body can be calculated by

$$\Delta U_{wd} = \int_{\eta_{wc}}^{\eta_{wa}} F_w(\eta_w)\mathrm{d}\eta_w. \tag{4}$$

The elastic energy released by the weak body is

$$\Delta U_{we} = \frac{1}{2}\frac{F^2(\eta_{wa})}{K_{wa}} - \frac{1}{2}\frac{F^2(\eta_{wc})}{K_w}, \tag{5}$$

where K_{wa} and η_{wa} refer to elastic modulus and displacement, respectively, at loading point a of the weak body.

Due to the stiffness deterioration at the postpeak stage, $K_{wa} < K_w$. In this process, the strong body is still at the elastic stage and will be unloaded to point a along the initial elastic loading line. The elastic energy released can be calculated by

$$\Delta U_{se} = \frac{1}{2}\frac{F_s^2(\eta_{sa})}{K_s} - \frac{1}{2}\frac{F_s^2(\eta_{sc})}{K_s}. \tag{6}$$

The external work can be calculated by

$$\Delta W = \int_{\eta_{tc}}^{\eta_{ta}} F_t\mathrm{d}\eta_t. \tag{7}$$

Based on energy conservation,

$$\Delta U_{se} + \Delta U_{we} + \Delta U_{wd} - \Delta W = 0. \tag{8}$$

Substituting equations (4)~(7) into (8),

$$\begin{aligned}&\frac{1}{2}\frac{F_s^2(\eta_{sa})}{K_s} - \frac{1}{2}\frac{F_s^2(\eta_{sc})}{K_s} + \frac{1}{2}\frac{F_w^2(\eta_{wa})}{K_{ma}}\\ &- \frac{1}{2}\frac{F_w^2(\eta_{wc})}{K_m} + \int_{\eta_{wc}}^{\eta_{wa}} F_w(\eta_w)\mathrm{d}\eta_w - \int_{\eta_{tc}}^{\eta_{ta}} F_t\mathrm{d}\eta_t = 0.\end{aligned} \tag{9}$$

As catastrophic damages occur in the weak body, its displacement η_w is regarded as the state variable of the system so that the displacement and load of the strong body are functions of η_w at the postpeak stage. Based on the variation principle, equation (9) can be rewritten as

$$F_w(\eta_w)\left[\left(\frac{1}{K_s} + \frac{1}{K_{wa}}\right)F_w'(\eta_w) + 1\right] = F_t(\eta_t)\frac{\delta\eta_t}{\delta\eta_w}. \tag{10}$$

2.3. Instability Failure Criterion of Strong-Weak Geological System. Let $J_0 = F_t(\eta_t)(\delta\eta_t/\delta\eta_w) = (\delta W/\delta\eta_w)$ be the energy input rate. Its physical meaning is that the energy required to be applied externally for unit deformation of the weak body produces $\delta\eta_w$. Hence, equation (10) is rewritten as

$$J_0 = F_w(\eta_w)\left[\left(\frac{1}{K_s} + \frac{1}{K_{wa}}\right)F_w'(\eta_w) + 1\right], \tag{11}$$

where $F_w'(\eta_w)$ refers to the tangent stiffness of the weak body at the postpeak strain softening stage.

Obviously, J_0 is a variable at the strain-softening stage. If $J_0 \longrightarrow 0$, external energy is not required and increasing deformation of the weak body can be achieved by the elastic energy released by the strong body and the weak body. This indicates that the system is not stable and catastrophic fractures tend to be observed. In this case,

$$F_w'(\eta_w) + \frac{1}{\left((1/K_s) + (1/K_{wa})\right)} = 0. \tag{12}$$

Equation (12) is the stiffness instability criterion of the strong-weak geological system.

However, the stiffness criterion of rock instability proposed by Cook is

$$f'(u_j) + k_m = 0, \tag{13}$$

where k_m refers to the tester stiffness and j refers to the starting point of the rock instability fracture. $f'(u_j)$ refers to the tangent slope of point j at the softening stage.

Let

$$\frac{1}{K_0} = \left(\frac{1}{K_s} + \frac{1}{K_{wa}}\right). \tag{14}$$

Equation (12) can be rewritten as

$$F_w'(\eta_w) + K_0 = 0. \tag{15}$$

As shown in equations (12) and (15), the stiffness criterion of instability failure proposed in this study is consistent with that by Cook. However, the elastic energy released from the weak body during fracturing is considered in the proposed model. Therefore, the equivalent stiffness K_0 of the interaction system includes not only the stiffness of the strong body but also the deteriorating stiffness of the weak body at the softening stage, which is equivalent to the loading stiffness of the tester in Cook's equation. As $K_0 < K_s$ and $K_0 < K_{wa}$, the catastrophic point of the instability failure of the weak body in this model is beyond the one in the model proposed by Cook. The system can be in two states before and after a sudden dynamic instability: the instability

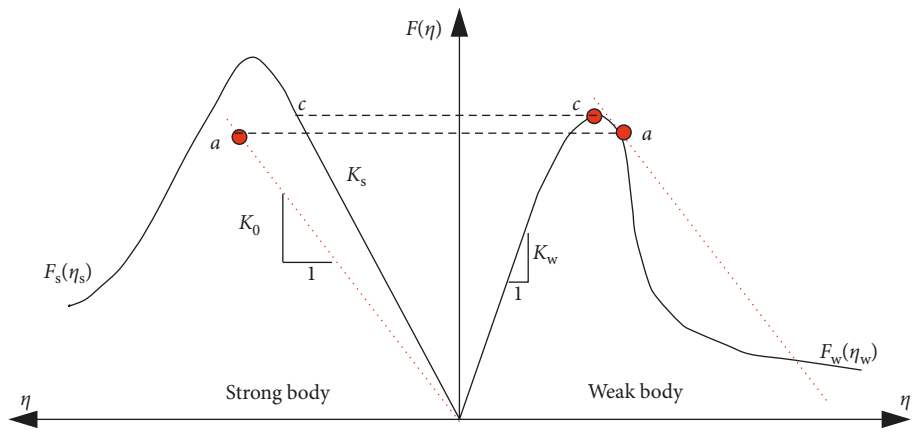

Figure 2: Load-displacement curves of the strong-weak geological system.

equilibrium state at the precursory stage of instability and a new stability equilibrium state after loading. For soft rocks with significant strain-softening behaviors, the catastrophic point may occur repeatedly due to their complicated softening. As a result, soft rocks are in the process of alternating stable and unstable deformations, as shown in Figure 3.

With a given $\Delta F_t(\eta_s)$, displacement increments in strong and weak body can be calculated by

$$\Delta\eta_s = \frac{\Delta F_s(\eta_w)}{F_s'(\eta_w)}, \qquad \Delta\eta_w = \frac{\Delta F_w(\eta_w)}{F_w'(\eta_w)}. \tag{16}$$

The total displacement increment of the system is

$$\Delta\eta_t = \Delta\eta_s + \Delta\eta_w. \tag{17}$$

As $\Delta F_s(\eta_s) = \Delta F_w(\eta_w) = \Delta F_t(\eta_w)$, equations (16) and (17) lead to

$$\begin{aligned} F_w'(\eta_w)\Delta\eta_w &= F_s'(\eta_s)(\Delta\eta_t - \Delta\eta_w), \\ F_w'(\eta_w)(\Delta\eta_t - \Delta\eta_s) &= F_s'(\eta_s)\Delta\eta_s. \end{aligned} \tag{18}$$

The deformation rates of strong body and weak body can be expressed as

$$\dot\eta_s = \frac{F_w'(\eta_w)}{F_w'(\eta_w) + F_s'(\eta_s)}\dot\eta_t, \qquad \dot\eta_w = \frac{F_s'(\eta_s)}{F_w'(\eta_w) + F_s'(\eta_s)}\dot\eta_t, \tag{19}$$

where η_t is the loading rate of the interaction system and it can be regarded as a constant. $F_s'(\eta_s)$ is the tangent slope of loading curve of strong body and should be substituted by K_0. Therefore, equation (19) shall be rewritten as

$$\dot\eta_s = \frac{1}{1 + (K_0/F_w'(\eta_w))}\dot\eta_t, \qquad \dot\eta_w = \frac{1}{(F_w'(\eta_w)/K_0) + 1}\dot\eta_t. \tag{20}$$

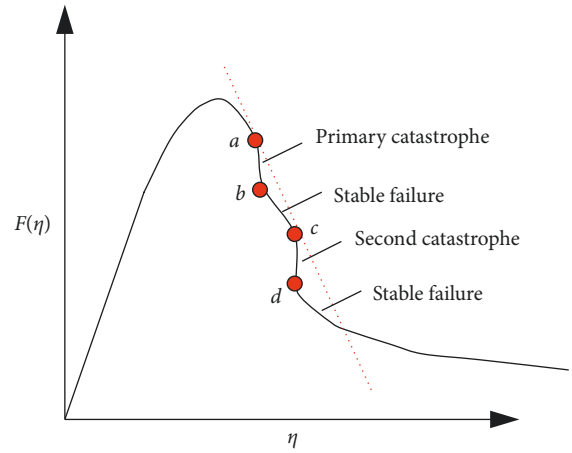

Figure 3: Catastrophic failures of rocks at postpeak stage.

According to equation (15), if $F_w'(\eta_w) \longrightarrow -K_0$, then $\dot\eta_s \longrightarrow \infty$ and $\dot\eta_w \longrightarrow \infty$. The instability failure is proportional to the consistency of these two parameters. Therefore, sudden changes in deformation rates of the two bodies can be regarded as the precursory information for catastrophic failures of the system.

3. Precursor Information of Instability Failure in Coal-Rock Body by Numerical Simulations

In order to fully understand the stiffness effect on failures of soft rock-coal body and demonstrate the feasibility of regarding deformation rate as precursory information of instability failure, the model was verified using numerical simulations based on relevant experiments.

3.1. Computational Model. A standard cylinder with diameter of 50 mm and height of 100 mm was constructed. Let the height ratio of rock and coal be 1 (Figure 4); the simulation was performed under uniaxial compressions. The particles on the upper and lower surfaces of the model were

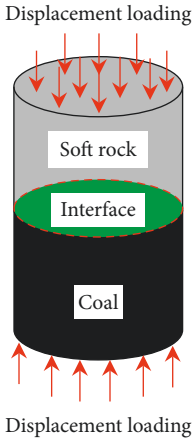

Figure 4: Compression model of coal-rock body.

allowed to move vertically only. Loads were applied by displacement control method at a rate v of 2×10^{-8} per step. The physical and mechanical parameters of rock and coal are listed in Table 1.

To fully understand the failure characteristics of strain-softening materials, the M-C ideal elastoplastic model and strain-softening model were employed for numerical calculations, and the results were compared with each other. In the M-C ideal elastoplastic model, the cohesion and the friction angle remain constant after yielding of elements. In the strain-softening model, however, strength parameters degraded after yielding of elements. According to relevant experimental results, the strength parameters of rock and coal attenuated at postpeak stage, as shown in Figure 5.

In the constitutive model of coal-rock body, elastoplastic-elastoplastic (M-M), elastoplastic-strain softening (M-S), and strain softening-strain softening (S-S) constitutive relations are observed. To guarantee uniform distribution of unit meshes and reasonable comparability of different constitutive models, the coal and rock were placed in the same grid system and divided into grids uniformly. It is assumed that the body interface exhibits high bonding strength with parameters as follows: normal stiffness and tangential stiffness $k_n = k_s = 300$ GPa/m, cohesion $C_c = 100$ MPa, and friction angle $\phi_c = 40^\circ$. Owing to effects of strain localization (concentration of deformations and failures in a localized region), stress-strain curves of ideal elastoplastic model also declined at the postpeak stage. To avoid that, the mesh size shall not be oversmall in order to achieve uniform unit deformation. The numerical calculation mesh is as follows: the system was divided into 10 elements along the radial direction and 20 elements along the axial direction. Each element is in size of 5 mm.

Figure 6 illustrates the stress-strain curves of coal-rock body in different constitutive models. As observed, the uniaxial compressive strength of the system was 13 MPa in the M-M model and 11.5 MPa in both M-S model and S-S model. In terms of the entire deformation process, the stress-strain relations in the three models coincide completely at the prepeak elastic stage, while their nonlinear deformation characteristics were significantly different. In the M-M

Table 1: Physicomechanical parameters of specimens.

Medium	Elastic modulus (GPa)	Poisson ratio	Initial cohesion (MPa)	Initial friction angle (°)	Tensile strength (MPa)
Soft rock	2.1	0.252	3.5	44	1.11
Coal	1.5	0.272	2.5	40	0.5

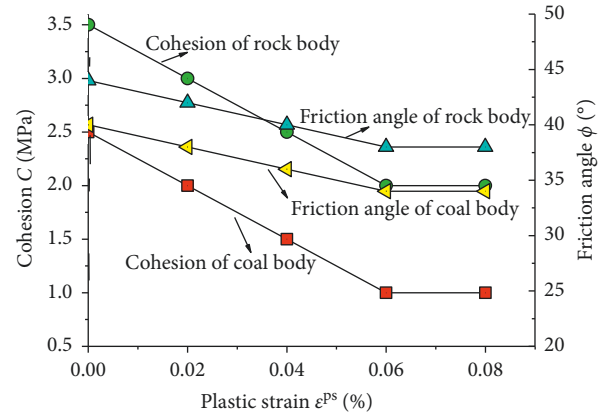

Figure 5: Attenuation of strength parameters of coal and rock at softening stage.

model, the strain increased rapidly upon reaching the peak strength, while the stress remained constant, which is typical ideal elastic-plastic deformation. In M-S model and M-M model, significant stress degradations were observed at the postpeak stage owing to increasing deformation as strength attenuation at postpeak stage was taken into consideration. Additionally, the stress degradation was proportional to the medium softening. For instance, the stress degradation modulus of the S-S model was larger than that of the M-S model.

In numerical simulations, failures start from one single element. Hence, the computational scale depends on the element size, and the computational time step is determined by the quantity of elements. In regions with high and concentrated maximum imbalance forces, element failures are readily observed. Based on that, the failure process of the model can be described, and the precursor information can be captured. As shown in Figure 6, the maximum imbalance forces varied smoothly during deformation and failure of M-M and M-S models, indicating progressive failures of the element. In the S-S model, the maximum unbalanced forces varied violently at the postpeak stress drop stage and several sudden increasing/decreasing cycles were observed, indicating sharp element failure at this stage and the failure concentration in one specific region (localized localization). In this study, the S-S model should be employed.

3.2. Computational Results. The stiffness ratio is defined to be $\alpha = E_r/E_m$, where E_r and E_m are elastic moduli of rock and coal, respectively. With other parameters being constant, the failure characteristics of coal-rock body as a function of the

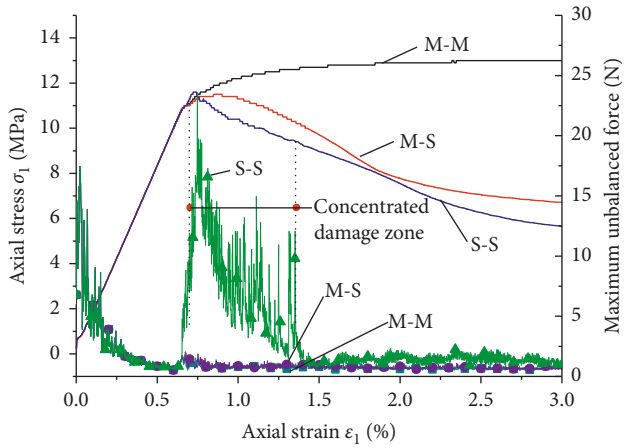

Figure 6: Stress-strain curves of coal-rock body in different constitutive models.

stiffness ratio α can be revealed by varying E_r. Two monitoring points were arranged at the middle element node near the contact surface on each body. Figure 7 shows the correlation of stress evolution of the two-body system and deformations measured at the monitoring points at different stiffness ratios. Owing to the effects of contact surface and the stiffness difference, deformation rates of coal and body are severely inconsistent and fluctuated significantly at the postpeak strain-softening stage. In terms of the stress evolution, a significant stress degradation was observed at $\alpha = 1$, demonstrating unexpectedness and instability of coal-rock system failures. This can be attributed to the fact that coal reaches its peak strength, while the rock body is still in the elastic stage. Like the loading system in the tester, the elastic energy of the rock at postpeak stage of the coal body is suddenly released due to the insufficient rock rigidity, resulting in shocking to the coal body. As α increased, the prepeak stiffness of the model was enhanced, and the postpeak stress degradation modulus dropped (smooth stress curve), demonstrating significant strain-softening behaviors. If $\alpha > 1$, the stress curve fluctuates and the fluctuation frequency is proportional to the stiffness ratio, demonstrating gradual and severe localizations during the failure process.

Figure 8 shows the ultimate failure modes of coal-rock body under different stiffness ratios. As strengths of coal and rock are highly consistent, a single shear band through the contact surface was observed at $\alpha = 1$. At $\alpha = 7$, two conjugated shear bands were generated by the intersection of interfaces. At $\alpha = 20$, no shear bands were observed in the coal body, illustrating overall plastic deformation. Additionally, the overall compressive plastic deformation of rock body was also observed in the vicinity of the contact area, and two shear bands with different thicknesses were generated starting from the middle part of the contact surface.

3.3. Results and Discussion. As α increased, the deformation rates of rock and coal exhibited two patterns.

First, the deformation rate exhibits a sudden drop near the peak point. The sudden drop was before the peak point at $\alpha = 1$ and after the peak point at $\alpha > 1$. Then, the deformation rate fluctuated sharply at the softening stage and remained stable at the residual stage. The sudden drop of deformation rate of rock at the prepeak stage indicates rebound of its elastic deformation to the coal body, namely, sudden release of elastic deformation energy from rock to coal. The sudden drop of deformation rate of coal indicates microfractures in the coal body, resulting in deformation instability. In fact, another sudden jump point of deformation rate was observed near the residual stage. According to the results, the failure of the coal-rock body is directly related to the deformation rates of coal and rock. The sudden drop points of coal and rock exhibit the feature of simultaneous fluctuation in one direction, and their position may vary due to the stiffness effect. Damage precursor information of coal-rock body can be captured based on the sudden drop of deformation rate. The first point is the starting point of the main fracturing of two-body system and can be regarded as the precursor information of the model failure; the second point is the breakthrough point of the main fracturing of two-body system. The fluctuations can be readily identified as they are highly frequent during the fluctuation section. The fluctuation frequency of the second point was significantly higher than that of the first point. For rock failures, a direct reflection of system instability is the maximum deformation rate.

Second, the fluctuation frequency of deformation rate in rock body decreased gradually as the stiffness increased. At $\alpha > 20$, the two sudden jumps in rock were eliminated, meaning that the rock has no shock effect on coal, and the coal-rock body exhibits stability failure. However, the first point was still observed in the coal body, indicating that the failure occurs in the coal body first under loading. As shown in Figure 7, the second point of coal body is independent of the stiffness ratio at $\alpha < 9$. This can be attributed to the fact that deformation localization in the model initiates from the coal body and the complexity of shear band caused by localization as a function of stiffness. However, the second point of the coal body was also eliminated at $\alpha = 30$, indicating overall plastic deformation of the two-body system, and no main fracture band was presented.

In summary, the failure characteristics of the coal-rock body system are directly related to the stiffness ratio of rock body and coal body. With stiffnesses of rock body and coal body being highly consistent, stress degradation was observed during stress evolution, and instability failure was observed. With stiffnesses of rock body and coal body being highly inconsistent, significant strain-softening behaviors were observed, and the model exhibited progressive stability failure. The composite model was exposed to overall plastic deformations. In weak cementation soft rock strata in western China, instability and sudden failures of surrounding rocks are readily observed due to consistent stiffnesses of soft rocks and coal. Although not as intense as those of hard rocks, these failures have a significant effect on the stability of soft rock roadway. In summary, although varying with the elastic modulus of coal and rock, the two points reflecting the failure information are readily

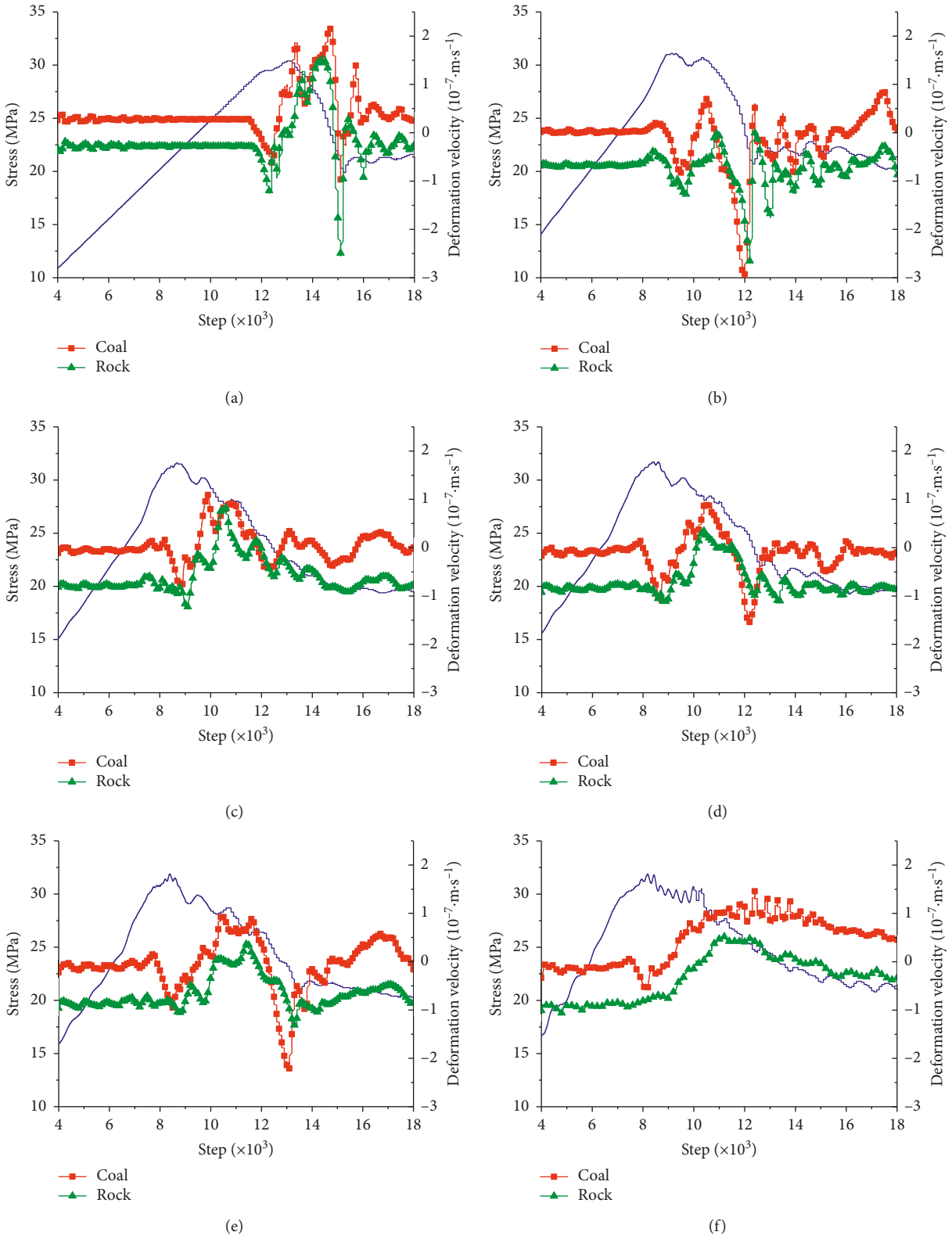

Figure 7: Stress evolution in deformation process of coal and rock. (a) $\alpha = 1$. (b) $\alpha = 3$. (c) $\alpha = 5$. (d) $\alpha = 7$. (e) $\alpha = 9$. (f) $\alpha = 20$.

identified and tested. Hence, the instability sudden failures of surrounding rocks can be predicted by monitoring the deformation rates of composite roof consisting of coal seams and rock layers in practical engineering.

4. Engineering Application

Located on the slope belt of southern margin of the Yili Basin in Xinjiang, the Yili No. 1 mine field has coal seams whose

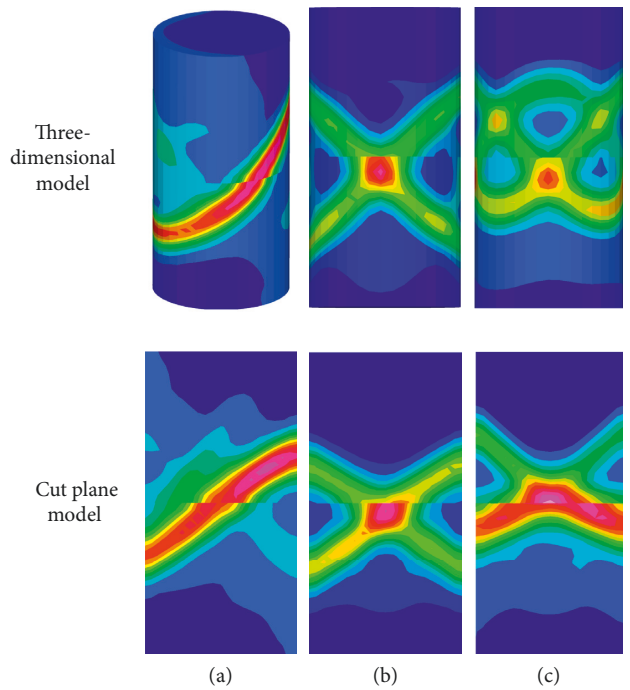

Figure 8: Failure modes of coal-rock body as a function of the stiffness ratio. (a) $\alpha = 1$. (b) $\alpha = 7$. (c) $\alpha = 20$.

roof and floor are mostly weakly cemented mudstone and argillaceous sandstone with low strength, weak cementation, and poor disturbance resistance. Therefore, roadways are often arranged in relatively stable coal seams, resulting in a typical coal-rock composite roof structure. However, working face excavation is often accompanied by weak roof shocking and the following characteristics are observed: (1) roof shocking is usually observed in coal bodies with good integrity, compacted structure, reduced crack propagation, and brittleness. (2) The roadway with roof shocking tends to be dry, and water drenching directly along the bolt, tray, and roof is seldom observed. (3) The roof shocking tends to be observed in a few hours or a few days after the head-on cut, and the frequency of roof shocking is inversely proportional to the distance of head-on. (4) In presence of intense roof shocking, bolt and tray may be loose, but the bolt does not shock out (Figure 9). Although not comparable to impact pressure, the roof shocking has a significant effect on the stability of surrounding rocks, thus the construction safety.

Four mining pressure observation stations were designed along the three coalbelt downhill roadways, and locations of roof measuring points are illustrated in Figure 10. The displacement meters were installed in rock stratum and coal seam near the coal-rock interface. By the method discussed in Section 3, the information of instability failures of surrounding rocks can be captured by monitoring deformations of roof seams and rock strata.

Figure 11 shows the deformation rates of rock strata and coal seams monitored. The roadway deformation can be divided into the roadway excavation stage, the deformation limit stage, and stable deformation stage as the workface excavation progresses. The effects of excavation unloading on surrounding rocks are reflected as rapid release of elastic

Figure 9: Anchorage system failure induced by roof shocking.

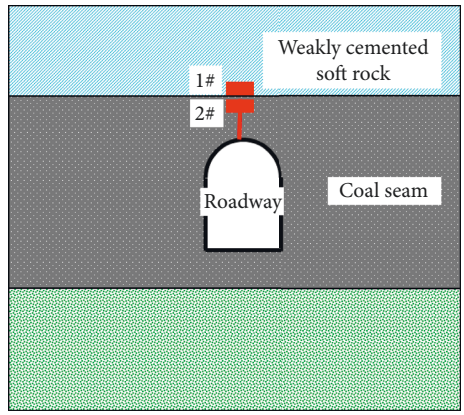

Figure 10: Monitoring of displacements of roof and floor.

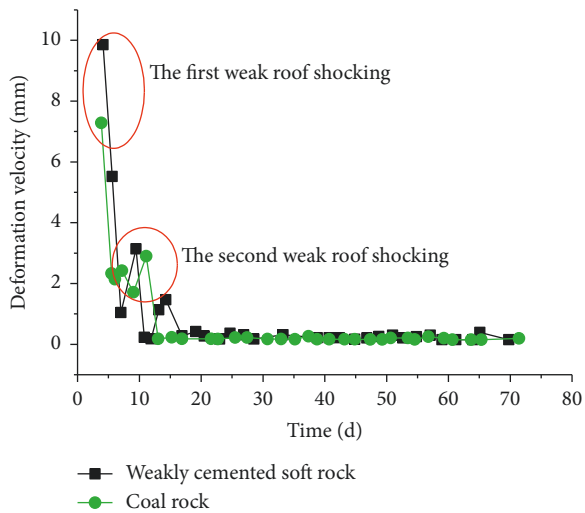

Figure 11: Deformation rates in coal and rock monitored.

deformation energy and high initial deformation rate. In order to avoid large deformations of surrounding rocks, the anchor net supports were arranged right after excavation. As observed in Figure 11, the deformation rate of surrounding rocks is relatively high in the first 10 days, and two sudden

jumps of deformations were observed in coal seam and rock stratum. Practically, roof shocking basically occurred at the observation point of sudden jumps, which is also the moment when the bolt support structure is readily exposed to damages. After redistribution of deformation and stress in the supporting system, coupled deformation of surrounding rock and supporting structure is realized, and the supporting system tends to be in equilibrium state. Owing to the rheological characteristics of soft rocks, the equilibrium is achieved gradually. According to monitoring data and the practical situation of surrounding rocks, it is reasonable to adopt the sudden jump of deformation rate of rock-coal structure as the precursory information of instability failures induced by weak roof shocking.

5. Conclusions

Aimed at weak roof shocking in weakly cemented soft rock stratum in mining engineering of western China, the mechanism of instability failures was investigated based on the overall bearing characteristics of the composite roof consisting of weak cemented soft rock and coal. The precursory information of weak shocking failures of rock-coal body was proposed based on theoretical analysis and numerical calculations. Industrial applications demonstrated good applicability and accuracy of the proposed approach. The following conclusions can be drawn:

(1) The failure of composite structure is initiated at the postpeak stage of weak geologic body, and the strain softening of rock mass is prerequisite for sudden catastrophic failures. Likewise, the weak body also releases elastic energy at the postpeak failure stage. According to the energy evolution in failure process of strong-weak body, the elastic energy released by the weak body at the postpeak stage also contributes to the failure of the composite structure. Therefore, the criterion for the instability failure of strong-weak system is consistent with the stiffness criterion proposed by Cook. However, the equivalent stiffness in the proposed model consists of both the stiffness of strong body and the deterioration stiffness of weak body at the softening stage.

(2) The critical point of instability failures of strong-weak structure is earlier than that in the stiffness criterion proposed by Cook. The critical points may appear repeatedly in weak cemented soft rocks at the postpeak stage, and the system is in the alternating process of steady state and unsteady state.

(3) In the proposed model, synchronous jumps of deformation rates in coal body and rock body can be recognized as the precursory information of catastrophes. The first sudden jump point is the starting point of the main fracturing, which can be regarded as the precursor information; the second sudden jump point is the breakthrough point of the main fracturing. The amplitudes of sudden jumps are significantly affected by stiffness. With large stiffness ratio of coal and rock, the two sudden jump points are eliminated, indicating that the strong body has no shock effect on the weak body and the system is exposed to stability failures.

(4) For coal mines in western China, the stiffness of weak cemented soft rock is highly consistent with that of coal body, and the composite roof is exposed to instability failures. This is referred as roof shocking, which is confirmed by field monitoring and practical cases. The results proposed can be applied to the study of rock burst and impact pressure in the softening rock system under different structures and loadings. According to the results of the theoretical model, numerical simulation, and field monitoring, it is feasible to use the jump of deformation rate as the precursor information of instability failures. However, further studies are still needed, especially laboratory tests.

Data Availability

The calculation data used to support the findings of this study are included within the article.

Conflicts of Interest

The authors declare that they have no conflicts of interest.

Acknowledgments

This work was supported by the National Key R&D Program of China (2018YFC0604702), National Natural Science Foundation of China (grant nos. 51774196 and 51578327), National Natural Science Foundation of China and Shandong Province Joint Program (U1806209), China Postdoctoral Science Foundation (no. 2016M592221), and SDUST Young Teachers Teaching Talent Training Plan (no. BJRC20160501).

References

[1] Y. D. Jiang and Y. X. Zhao, "State of the art: investigation on mechanism, forecast and control of coal bumps in China," *Chinese Journal of Rock Mechanics and Engineering*, vol. 34, no. 11, pp. 2188–2204, 2015.

[2] H. Lippmann, "Mechanics of "bumps" in coal mines: a discussion of violent deformations in the sides of roadways in coal seams," *Applied Mechanics Reviews*, vol. 40, no. 8, pp. 1033–1043, 1987.

[3] H. P. Wu, Z. H. Chen, H. W. Zhou, C. Yi, and Z. J. Chen, "Study on two-body mechanical model based on interaction between structural body and geo-body," *Chinese Journal of Rock Mechanics and Engineering*, vol. 24, no. 9, pp. 1464–1487, 2005.

[4] I. M. Petukhov and A. M. Linkov, "The theory of post-failure deformations and the problem of stability in rock mechanics," *International Journal of Rock Mechanics and Mining Sciences & Geomechanics Abstracts*, vol. 16, no. 2, pp. 57–76, 1979.

[5] X. B. Wang, "Numerical simulation of deformation and failure for two bodies model composed of rock and coal," *Rock and Soil Mechanics*, vol. 27, no. 7, pp. 1066–1070, 2006.

[6] X. N. Wang, C. P. Lu, J. H. Xue et al., "Experimental research on rules of acoustic emission and microseismic effects of burst failure of compound coal-rock samples," *Rock and Soil Mechanics*, vol. 34, no. 9, pp. 2569–2575, 2013.

[7] J. Liu, E. Y. Wang, D. Z. Song et al., "Effects of strength on mechanical behavior and acoustic emission characteristics of samples composed of coal and rock," *Journal of China Coal Society*, vol. 39, no. 4, pp. 685–691, 2014.

[8] Z. L. Mu, H. Wang, P. Peng et al., "Experimental research on failure characteristics and bursting liability of rock-coal-rock sample," *Journal of Mineral Safety Engineering*, vol. 30, no. 6, pp. 841–847, 2013.

[9] J. Zuo, Z. Wang, H. Zhou, J. Pei, and J. Liu, "Failure behavior of a rock-coal-rock combined body with a weak coal interlayer," *International Journal of Mining Science and Technology*, vol. 23, no. 6, pp. 907–912, 2013.

[10] J. P. Zuo, Y. Chen, Y. J. Sun et al., "Investigation on whole failure nonlinear model for deep coal-rock combined bodies," *Journal of Mining Science and Technology*, vol. 2, no. 1, pp. 17–24, 2017.

[11] X. L. Li, L. J. Kang, H. Y. Li, and Z. H. OuYang, "Three-dimensional numerical simulation of bust-prone experiments about coal-rock combination," *Journal of China Coal Society*, vol. 36, no. 12, pp. 2064–2067, 2011.

[12] Q. X. Qi, *Theory of rock burst caused by structure failure of bedded coal rock mass and its application*, Ph.D. thesis, Beijing Mining Research Institute, China Coal Research Institute, Beijing, China, 1996.

[13] S. Qin, J. J. Jiao, C. A. Tang, and Z. Li, "Instability leading to coal bumps and nonlinear evolutionary mechanisms for a coal-pillar-and-roof system," *International Journal of Solids and Structures*, vol. 43, no. 25-26, pp. 7407–7423, 2006.

[14] L. X. Wu and J. Z. Wang, "Features of infrared thermal image and radiation temperature of coal rocks loaded," *Science in China Series D*, vol. 28, no. 2, pp. 41–46, 1998.

[15] L. Wu and J. Wang, "Infrared radiation features of coal and rocks under loading," *International Journal of Rock Mechanics and Mining Sciences*, vol. 35, no. 7, pp. 969–976, 1998.

[16] L. Wu, S. Liu, Y. Wu, and H. Wu, "Changes in infrared radiation with rock deformation," *International Journal of Rock Mechanics and Mining Sciences*, vol. 39, no. 6, pp. 825–831, 2002.

[17] Y. F. Dong, B. Yu, F. S. Hao et al., "An experimental research on the infrared radiation in coal rupture," *Journal of Experimental Mechanics*, vol. 17, no. 2, pp. 206–211, 2002.

[18] Y. X. Zhao, Y. D. Jiang, and Z. R. Han, "Experimental study on acoustic and thermal infrared characteristics of bump-prone coal," *Chinese Journal of Rock Mechanics and Engineering*, vol. 26, no. 5, pp. 965–971, 2007.

[19] Y. Zhao and Y. Jiang, "Acoustic emission and thermal infrared precursors associated with bump-prone coal failure," *International Journal of Coal Geology*, vol. 83, no. 1, pp. 11–20, 2010.

[20] Y. X. Zhao, Y. D. Jiang, J. Zhu, and G. Z. Sun, "Experimental study on precursory information of deformations of coal-rock composite samples before failure," *Chinese Journal of Rock Mechanics and Engineering*, vol. 27, no. 2, pp. 339–346, 2008.

[21] X. Z. Lyu, Z. H. Zhao, X. J. Wang, and W. M. Wang, "Study on the permeability of weakly cemented sandstones," *Geofluids*, vol. 2019, article 8310128, 14 pages, 2019.

[22] Z. H. Zhao, W. M. Wang, and X. Gao, "Evolution laws of strength parameters of soft rock at the post-peak considering stiffness degradation," *Journal of Zhejiang University Science A*, vol. 15, no. 4, pp. 282–290, 2014.

[23] Z. Zhao, W. Wang, L. Wang, and C. Dai, "Compression-shear strength criterion of coal-rock combination model considering interface effect," *Tunnelling and Underground Space Technology*, vol. 47, pp. 193–199, 2015.

[24] Z. Zhao, Q. Ma, Y. Tan, and X. Gao, "Load transfer mechanism and reinforcement effect of segmentally yieldable anchorage in weakly consolidated soft rock," *Simulation*, vol. 95, no. 1, pp. 83–96, 2019.

[25] N. G. W. Cook, "The failure of rock," *International Journal of Rock Mechanics and Mining Sciences & Geomechanics Abstracts*, vol. 2, no. 4, pp. 389–403, 1965.

[26] C. A. Li, *Catastrophe in Rock Fracture*, pp. 20–25, China Coal Industry Publishing House, Beijing, China, 1993.